Structure of flexible and semiflexible polyelectrolyte chains in confined spaces of slit micro/nanochannels

Jonggu Jeon and Myung-Suk Chun[a)]
Complex Fluids Research Laboratory, Korea Institute of Science and Technology (KIST), Seoul 136-791, Republic of Korea

(Received 18 January 2007; accepted 14 March 2007; published online 19 April 2007)

Understanding the behavior of a polyelectrolyte in confined spaces has direct relevance in design and manipulation of microfluidic devices, as well as transport in living organisms. In this paper, a coarse-grained model of anionic semiflexible polyelectrolyte is applied, and its structure and dynamics are fully examined with Brownian dynamics (BD) simulations both in bulk solution and under confinement between two negatively charged parallel plates. The modeling is based on the nonlinear bead-spring discretization of a continuous chain with additional long-range electrostatic, Lennard-Jones, and hydrodynamic interactions between pairs of beads. The authors also consider the steric and electrostatic interactions between the bead and the confining wall. Relevant model parameters are determined from experimental rheology data on the anionic polysaccharide xanthan reported previously. For comparison, both flexible and semiflexible models are developed accompanying zero and finite intrinsic persistence lengths, respectively. The conformational changes of the polyelectrolyte chain induced by confinements and their dependence on the screening effect of the electrolyte solution are faithfully characterized with BD simulations. Depending on the intrinsic rigidity and the medium ionic strength, the polyelectrolyte can be classified as flexible, semiflexible, or rigid. Confined flexible and semiflexible chains exhibit a nonmonotonic variation in size, as measured by the radius of gyration and end-to-end distance, with changing slit width. For the semiflexible chain, this is coupled to the variations in long-range bond vector correlation. The rigid chain, realized at low ionic strength, does not have minima in size but exhibits a sigmoidal transition. The size of confined semiflexible and rigid polyelectrolytes can be well described by the wormlike chain model once the electrostatic effects are taken into account by the persistence length measured at long length scale. © *2007 American Institute of Physics*. [DOI: 10.1063/1.2723091]

I. INTRODUCTION

When polyelectrolytes exist in confined spaces with either nano- or micrometer scale, they exhibit some or all different behaviors compared to the bulk solution due to interactions with the bounding surfaces.[1–3] Understanding this confinement effect has direct relevance in such research fields as microfluidics, lab on a chip, and manipulations in the micro total analysis system (μTAS). It is also of fundamental importance in the biological science since many life phenomena involve transport of charged biopolymers in confined environment.

In general, confined polymers exhibit a transition from unperturbed three-dimensional (3D) behavior to that in reduced dimensions.[4,5] Thus, Daoud and de Gennes scaling theory[4,6] predicts that the end-to-end distance R_E of a self-avoiding polymer with N monomers of size a scales as $N^{3/4}a(a/W)^{1/4}$ in a narrow slit with width $W \ll R_E^{\text{bulk}}$, in contrast with the bulk scaling $R_E^{\text{bulk}} \sim aN^{3/5}$. A more elaborate variational theory by Cordeiro *et al.*[7] provides the prefactor to the scaling relation and, moreover, identifies a crossover regime between the strong and weak confinements where the chain size assumes a minimum. The location of the minimum depends on the strength of the polymer-surface repulsion and corresponds to $W/R_E^{\text{bulk}} \leqslant 1$. The same qualitative behavior has been observed in many different contexts such as lattice Monte Carlo simulations of a self-avoiding random walk chain between two parallel plates in dilute[8,9] and semidilute[9,10] regimes, Monte Carlo study of a bead-spring model in random porous media,[11] and a self-consistent perturbation theory of self-avoiding polymers in a cylindrical pore.[12] This indicates that nonmonotonic chain size variation with the degree of confinement is a universal phenomenon for flexible neutral polymers regardless of the type of confinement. For a self-avoiding chain between two parallel plates, van Vliet *et al.*[8,13] have shown that the confinement progresses in stages. As the slit narrows, the chain first orients itself so that its two longest axes are aligned with the walls, then contracts in all three principal directions, and finally, when $W/R_E^{\text{bulk}} \leqslant 1$, expands in two directions parallel to the walls while contracting in the perpendicular direction.

The above behavior applies to intrinsically flexible chains with the persistence length $l_P \approx a/2$ or semiflexible chains at length scales much larger than l_P. For a semiflexible (or wormlike) chain with larger l_P, the finite flexibility needs to be taken into account. For a weakly confined chain in a pore with size $D > l_P$, its dimension R scales as $Na(al_P/D^2)^{1/3}$.[14] In contrast, we have $R \approx R_C[1-(l_D/l_P)/2]$

[a)]Author to whom correspondence should be addressed. Electronic mail: mschun@kist.re.kr

in the strong confinement limit with $D \ll l_P$, where R_C is the contour length and $l_D=(D^2 l_P)^{1/3}$ is the deflection length originally proposed by Odijk.[15,16]

In the present work, we investigate the behavior of a single polyelectrolyte chain confined in slit channels formed by two parallel plates with width ranging from several tens to thousands nanometers. Polyelectrolytes are distinguished from neutral polymers by the presence of charged groups with long-range electrostatic interactions. Additional complication arises from the screening of electrostatic interaction by ions always present in aqueous solution. These aspects hamper or prevent a direct application of powerful scaling theories developed for neutral polymers,[17,18] and it is usually necessary to consider more system-specific aspects such as the chain linear charge density, condensation of counterions and salt ions, the ionic strength of the solution, and Debye screening.

We first develop coarse-grained models of polyelectrolytes with polysaccharide xanthan[19,20] as the model system. Although its structure remains to be fully elucidated, xanthan is generally accepted as a semiflexible polyelectrolyte at room temperature due to the double stranded structure with intrinsic persistence length of at least 100 nm.[21–24] It has up to two ionizable carboxyl groups per repeat unit. To evaluate the effect of the intrinsic rigidity in addition to the stiffening due to electrostatic repulsion, two charged models with and without the angle bending potential are developed, representing the semiflexible and flexible polyelectrolytes, respectively. (In this paper, the term "semiflexible" is used to describe chains with nonzero persistence length. This includes chains with bending potentials and intrinsically flexible polyelectrolytes at low ionic strengths which have zero intrinsic persistence length but nonzero persistence length of electrostatic origin.) Based on a common first-order algorithm,[25] Brownian dynamics (BD) simulations of these models in bulk solutions and under confinement between parallel plates provide information on both conformational and dynamic behavior of a polyelectrolyte, especially including the confinement-induced changes. The strong influences of the medium ionic strength via the Debye-Hückel (DH) electrostatics and its interplay with the confinement effect are highlighted.

In the next two sections, the coarse-grained modeling of polyelectrolytes and the employed computational methods are described. The results of simulation are presented next for the bulk behavior and the changes due to confinement. These results are compared with predictions of the wormlike chain model, and conclusions are drawn in the final section.

II. COARSE-GRAINED MODELING OF XANTHAN POLYELECTROLYTE

We describe a polyelectrolyte molecule as a bead-spring chain with additional electrostatic, hydrodynamic, and Lennard-Jones (LJ) interactions between pairs of beads. Two models representing respectively an intrinsically flexible chain and an intrinsically semiflexible chain are developed. The flexible chain (model A) does not have the angle bending potential and thus its rigidity is solely due to the bead-bead electrostatic repulsion, while the semiflexible chain (model B) includes the bending potential between neighboring bonds. The potential functions and parametrization procedure are described in the following.

For the spring, the finitely extensible nonlinear elastic (FENE) potential[26] is employed to reflect the nonlinear relationship between the chain stress and the variation of the shape, expressed as

$$E_{i,i+1}^{\mathrm{FENE}} = -\left(\frac{k_S l_{\max}^2}{2}\right)\ln[1-(r_{i,i+1}-l_0)^2/l_{\max}^2], \tag{1}$$

where $r_{i,i+1}$ is the distance between beads i and $i+1$, l_0 is the equilibrium bond length, and $l_{\max}$ is the maximum bond length allowed. In the limit of large $l_{\max}$, E^{FENE} is reduced to a harmonic potential with force constant k_S.

The dispersion-repulsion interaction between beads are taken into account by the standard LJ potential

$$E_{ij}^{\mathrm{LJ}} = 4\varepsilon_{\mathrm{LJ}}[(\sigma_{\mathrm{LJ}}/r_{ij})^{12}-(\sigma_{\mathrm{LJ}}/r_{ij})^6], \tag{2}$$

where parameters $\varepsilon_{\mathrm{LJ}}$ and σ_{LJ} are set equal to the Boltzmann thermal energy k_BT and l_0, respectively. The electrostatic interaction between beads are described by the DH potential

$$E_{ij}^{\mathrm{ES}} = \frac{q_b^2}{4\pi\varepsilon}\frac{e^{-\kappa r_{ij}}}{r_{ij}} = k_B T z_b^2 \frac{l_B}{r_{ij}} e^{-\kappa r_{ij}}. \tag{3}$$

Here, q_b is the bead charge, $\kappa=(8\pi l_B N_A I)^{1/2}$ is the inverse Debye screening length defined in terms of Avogadro's number N_A and ionic strength I, $l_B=e^2/(4\pi\varepsilon k_B T)$ is the Bjerrum length ($l_B=0.71$ nm for water at $T=298$ K), $\varepsilon=\varepsilon_r\varepsilon_0$ is the dielectric constant of the medium defined in terms of relative dielectric permittivity ε_r and vacuum permittivity ε_0, and $z_b=q_b/e$ is the bead charge in units of positive elementary charge e. The finite rigidity of the chain is modeled by the following harmonic bending potential:

$$E_{i,i+1}^{\mathrm{bend}} = \tfrac{1}{2}k_A\theta_{i,i+1}^2, \quad \theta_{i,i+1}=\cos^{-1}(\hat{b}_i\cdot\hat{b}_{i+1}), \tag{4}$$

where k_A is the bending force constant and $\hat{b}_i=(\mathbf{r}_{i+1}-\mathbf{r}_i)/|\mathbf{r}_{i+1}-\mathbf{r}_i|$ is the ith bond vector of unit size.

The xanthan chain with molecular weight of 1.13×10^6 g/mol ($\sim$1220 monomers) has $l_P\cong120$ nm and the contour length $R_C\cong580$ nm at ionic strength $I=100$ mM.[24] Considering the ratio $R_C/l_P\approx5$, this chain can be regarded as a continuous wormlike chain. This is modeled as a discrete wormlike chain with 25 beads ($N_b=25$), with about ten beads representing a Kuhn segment of length $2l_P$. This choice ensures a smooth persistence length variation with changing environmental conditions. The bead hydrodynamic radius a is chosen as 5 nm. This is close to the value ranging 3–4 nm, which is determined by taking the experimentally estimated xanthan chain diameter of 2.2–4 nm (Refs. 22, 23, and 27) and then equating the volume of a cylinder of such diameter and 580 nm length to the volume of 25 beads.

In the flexible chain (model A), the bending potential is absent, and the spring and charge parameters k_S, l_0, $l_{\max}$, and q_b are optimized with short BD simulations so that the chain in bulk solution reproduces experimental values of $R_C=580$ and 880 nm at ionic strengths $I=100$ and 0.2 mM, respectively. Model B has a finite intrinsic rigidity and thus the

TABLE I. Input parameters of the intrinsically flexible (A) and semiflexible (B) models of xanthan polyelectrolyte and other simulation parameters.

	Model A	Model B
N_b	25	25
a (nm)	5.0	5.0
k_A (k_BT)	—	4.0
k_S (k_BT/l_0^2)	3.0	2.5
l_0 (nm)	18.0	10.0
$l_{\max}$ (nm)	40.0	150.0
q_b (e)	−30.0	−35.0
$\varepsilon_{\mathrm{LJ}}$ (k_BT)	1.0	1.0
σ_{LJ} (l_0)	1.0	1.0
σ_W (C/m^2)	-5.2×10^{-4}	-5.2×10^{-4}
k_W ($l_0^2k_BT$)	2.5	2.5
ε_r	78.4	78.4
η (mPa s)	0.89	0.89
T (K)	298.15	298.15
Δt (ns)	3.3	2.0

persistence lengths at the same I can also be reproduced by additionally adjusting k_A. The target values $l_P=120$ and 200 nm at $I=100$ and 0.2 mM are taken from the previous results of Chun and Park.[24]

The optimized model parameters are summarized in Table I. To reproduce a large change in R_C with I solely from the bead-bead electrostatic repulsion, the spring is required to be very weak and the optimal spring constants found as $k_S=2.5$ and $3.0k_BT/l_0^2$ are quite small. We note that a similarly large change in R_C (i.e., 450 and 1651 nm at $I=500$ mM and in pure water, respectively) has been reported from atomic force microscopy study on dehydrated samples.[28] This extension of xanthan at low ionic strength is likely to involve a structural transition from double strand to a disordered form with lower strandedness.[28,29] Thus, the weak spring constant employed here is not so much a signature of an entropic spring as a convenient way to take into account the large ionic strength dependence of xanthan contour length. The optimal bead charges q_b of −30 and $-35e$, also shown in Table I, are ~30% of the maximum possible value of $-98e$ for the bead composed of 49 (=1220/25) monomers. These lead to the contour distance per elementary charge $l_q[=R_C/(N_bz_b)]$ of 0.77 and 0.66 nm for models A and B, respectively, with the aforementioned target contour lengths at high ionic strength. According to the Manning condensation,[17,30] the minimum possible value of l_q in the presence of monovalent counterions is the Bjerrum length l_B (0.71 nm), in agreement with the above l_q values within 10%. Therefore, the parametrized bead charges can be regarded as already reflecting the possibility of counterion condensation, and it is not necessary to explicitly consider counterions. Finally, the optimized angle bending force constant was determined as $k_A=4k_BT$. This yields $l_P=4b$, where b indicates the average bond length, with the relation $l_P=bk_A/(k_BT)$ for a wormlike chain.[31–33] This is close to the simulation result, $l_P=4.3b$ at $I=100$ mM, if $b=2.4l_0$ determined from the same BD simulation is used. In this regard, model B behaves like a wormlike chain at high I.

In addition to the potentials between beads, the simulation of a confined chain requires the specification of the bead-wall interactions. For the bead-wall steric repulsion, the following empirical potential[34] is used:

$$E_i^{\mathrm{WR}}=k_W/(|z_i|-Z_0)^2, \tag{5}$$

with $k_W=2.5l_0^2k_BT$. For the electrostatics, we employ the DH interaction of a point charge with two infinite charged plates (E^{WES}) as follows:

$$E_i^{\mathrm{WES}}=\frac{q_b\sigma_W}{\varepsilon\kappa\sinh(\kappa Z_0)}\cosh(\kappa z_i)\cong\frac{2q_b\sigma_We^{-\kappa Z_0}}{\varepsilon\kappa}\cosh(\kappa z_i), \tag{6}$$

where σ_W is the wall charge density, Z_0 is the half-width of the slit, and z_i is the z coordinate of bead i with the z axis perpendicular to the walls and the origin at the center of the slit. This expression was obtained by solving the linearized Poisson-Boltzmann equation (i.e., DH approximation) with constant charge boundary condition at the walls. The approximation in the second relation above is valid because $\kappa Z_0>10$ in all cases studied here. The wall charge density σ_W is chosen as -5.2×10^{-4} C/m^2, comparable to the estimation from the zeta potential at pH 7, -5.8×10^{-4} and -1.03×10^{-3} C/m^2 for polydimethylsiloxane and glass surfaces, respectively.[35] For simplicity, we do not consider ionic strength dependence of σ_W.

III. COMPUTATIONAL METHODS

Note that the generalized Langevin equation provides the reference for the generation of molecular trajectories. The dynamics of the polyelectrolyte chain is described by the following BD equation of motion with account of the bead-bead hydrodynamic interaction:[25]

$$\mathbf{r}_i^{n+1}=\mathbf{r}_i^n+\Delta t\sum_j\frac{\mathbf{D}_{ij}^n\cdot\mathbf{F}_j^n}{k_BT}+\Delta t\sum_j\nabla_j\cdot\mathbf{D}_{ij}^n+\mathbf{R}_i^n, \tag{7}$$

where $\mathbf{D}_{ij}^n$ is the Rotne-Prager diffusion tensor, $\mathbf{F}_j^n=-\nabla E^{\mathrm{total}}(t_n)$ is the force on bead i at time step n, $\mathbf{R}_i^n$ is the random displacement due to the solvent, and Δt is the time step size. The hydrodynamic interaction between beads is described by the Rotne-Prager diffusion tensor[36]

$$\mathbf{D}_{ii}=\frac{k_BT}{6\pi\eta a}\mathbf{I},$$

$$\mathbf{D}_{ij}=\frac{k_BT}{8\pi\eta r_{ij}}\left[\left(\mathbf{I}+\frac{\mathbf{r}_{ij}\mathbf{r}_{ij}}{r_{ij}^2}\right)+\frac{2a^2}{r_{ij}^2}\left(\frac{1}{3}\mathbf{I}-\frac{\mathbf{r}_{ij}\mathbf{r}_{ij}}{r_{ij}^2}\right)\right]\quad(i\neq j,r_{ij}>2a), \tag{8}$$

$$\mathbf{D}_{ij}=\frac{k_BT}{6\pi\eta a}\left[\left(1-\frac{9}{32}\frac{r_{ij}}{a}\right)\mathbf{I}+\frac{3}{32}\frac{\mathbf{r}_{ij}\mathbf{r}_{ij}}{ar_{ij}}\right]\quad(i\neq j,r_{ij}\leqslant 2a),$$

where η is the solvent viscosity and $\mathbf{I}$ is the 3×3 unit tensor. The distribution of $\mathbf{R}_i^n$ is Gaussian with zero mean and covariance $\langle\mathbf{R}_i^n\mathbf{R}_j^n\rangle=2\mathbf{D}_{ij}^n\Delta t$. Integration time step Δt is chosen as 3.3 and 2.0 ns for models A and B, respectively. These values satisfy the condition[25] $m_0/(6\pi\eta a)\ll\Delta t\ll6\pi\eta a^3/k_BT$ (m_0 is the bead mass). In this study, the hydrodynamic inter-

action between the wall and the beads is not taken into account. This does not affect structures, but the diffusion of confined chains will only reflect conformational contribution. Full description of the bead-wall hydrodynamic interaction will be the subject of future work.

For a given condition, 20 independent BD trajectories are analyzed for each of more than 10 ms in length. Structural properties such as the chain radius of gyration R_G, root-mean-square end-to-end distance R_E, contour length R_C, and persistence length l_P are determined with the following formulas:[37]

$$R_G^2 = \frac{1}{N_b}\sum_{n=1}^{N_b} \langle |\mathbf{r}_n - \mathbf{r}_{\text{c.m.}}|^2 \rangle, \quad \mathbf{r}_{\text{c.m.}} = \frac{1}{N_b}\sum_{n=1}^{N_b} \mathbf{r}_n, \tag{9}$$

$$R_E = \langle \mathbf{R}_E^2 \rangle^{1/2}, \quad \mathbf{R}_E = \mathbf{r}_{N_b} - \mathbf{r}_1 = \sum_{n=1}^{N_b} \mathbf{r}_n, \tag{10}$$

$$R_C = (N_b - 1)b = \sum_{n=1}^{N_b-1} b_n = \sum_{n=1}^{N_b-1} |\mathbf{r}_{n+1} - \mathbf{r}_n|, \tag{11}$$

$$\frac{1}{N_b - n - 2}\left\langle \sum_{i=1}^{N_b-n-2} \hat{b}_i \cdot \hat{b}_{i+n} \right\rangle = \exp\left(\frac{-s_n}{l_P^n}\right),$$
$$s_n = \frac{1}{N_b - n}\left\langle \sum_{i=1}^{N_b-n} \sum_{m=1}^{n} |\mathbf{r}_{i+m} - \mathbf{r}_{i+m-1}| \right\rangle. \tag{12}$$

In these formulas, the position of the center of mass $\mathbf{r}_{\text{c.m.}}$, the average bond length b, the length of the nth bond b_n, and the average contour distance between beads separated by n bonds s_n are also introduced. It should be noted that the contour length R_C defined above can vary with medium ionic strength due to variable screening of bead-bead electrostatic interactions. When the bond vector correlation decays exponentially on the entire length scale, l_P^n becomes independent of n. As described above, l_P^n provides a useful measure of the relative strength of the short- and long-range bond vector correlations. Although the above expression for l_P^n involves all 25 beads in the chain, two terminal beads on each end of the chain are excluded in actual analysis to remove the chain end effect.

The translational self-diffusion coefficient is calculated from the Einstein relation

$$D_T^\alpha = \lim_{t\to\infty} \frac{1}{2t}\langle [r_{\text{c.m.}}^\alpha(t + t_0) - r_{\text{c.m.}}^\alpha(t_0)]^2 \rangle \quad (\alpha = x, y, z). \tag{13}$$

To better reveal the effect of confinement on diffusivity, we consider only the two-dimensional diffusion coefficients $D_T^{2D} = (D_T^x + D_T^y)/2$ both in bulk and under confinement. In practice, the limit $t \to \infty$ on the right-hand side of Eq. (13) is replaced by $t = 0.2$ ms. The estimated error from this choice is less than 2% in bulk solution and less than 5% under confinement.

TABLE II. Calculated structural parameters of the flexible (A) and semiflexible (B) model polyelectrolytes in the bulk solution at different ionic strengths I. All length scales are in nm.

I (mM)	R_G	R_E	R_C	l_P^1	l_P^{15}
			Model A		
100	35.0	66.9	581.2	0.0	38.5[a]
4	51.5	118.3	607.0	9.6	0.0
1	100.8	260.5	725.9	29.5	84.1
0.2	153.5	413.4	875.5	67.2	137.7
0.01	267.1	823.1	1033.5	276.3	824.1
			Model B		
100	116.4	315.5	573.9	105.3	108.5
4	125.4	341.5	619.6	113.1	119.9
1	146.7	402.5	719.6	134.9	151.7
0.2	188.5	530.9	867.8	197.3	225.5
0.01	295.7	919.6	1093.6	534.0	1075.5

[a]This nonzero value is likely due to a numerical error.

IV. RESULTS AND DISCUSSION

A. Properties in the bulk phase

The structure of polyelectrolyte chains depends sensitively on the medium ionic strength in bulk solution. Important structural parameters obtained from the simulation are summarized in Table II. Figure 1 depicts the radius of gyration R_G, the ratio $(R_E/R_G)^2$, and contour length R_C of each model in the bulk solution as a function of inverse Debye length κ. At κ larger than 0.5 nm^{-1} ($I \geqslant 20$ mM), the chain structure is nearly identical to that of the corresponding neutral chain. Due to the lack of intrinsic rigidity, model A exhibits a smaller size in this regime than model B. With $(R_E/R_G)^2 < 4$ at large κ [Fig. 1(b)], model A is even more collapsed than the ideal Gaussian chain, which has $(R_E/R_G)^2 = 6$.[37] With decreasing κ, the chain begins to extend due to electrostatic repulsion and structural parameters of each model converge to that of a fully extended chain. For example, $(R_E/R_G)^2 = 9.5$ and 9.7 for each model at $\kappa = 0.01$ nm^{-1} could be close to the value of 12 corresponding to the full extension. Figure 1(c) shows the variation of R_C with κ. The experimentally observed large increase of R_C with decreasing κ (Refs. 24 and 28) is well reproduced by both models.

The medium ionic strength also strongly influences the persistence length. According to Fig. 2 and Table II, the distance-dependent persistence length l_P^n shows a modest increase until the Debye screening length κ^{-1} reaches 21 nm ($I = 0.2$ mM), close to the average bond length of 24 nm, then rapidly increases to ~ 1 μm at $\kappa^{-1} \cong 100$ nm ($I = 0.01$ mM). Qualitatively, the behavior of l_P^n is similar between models A and B, except for the difference in the starting value at small κ^{-1} (i.e., 0 and 105 nm for models A and B, respectively). In Table II, l_P^{15} of model A exhibits a nonzero value of 38.5 nm at $I = 100$ mM. However, l_P^n of this chain at other length scales are all zero except at $n = 15$ and 19, which is likely due to a noise in the bond vector correlation function arising from the highly flexible nature of the chain. Thus, the persistence length of model A at high I can be regarded as zero, reflecting the lack of bending potential.

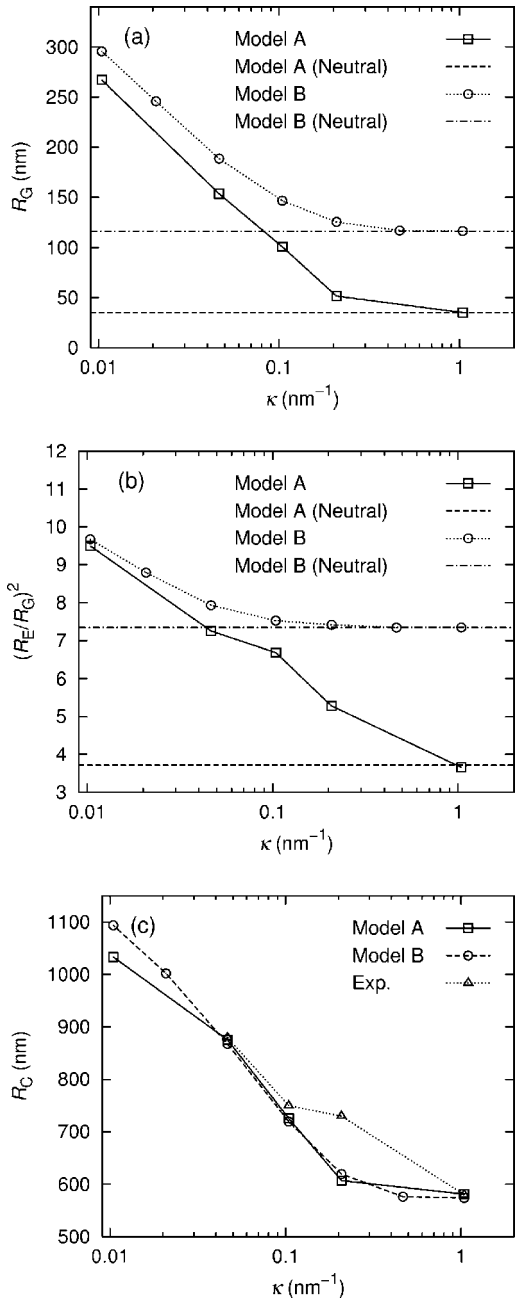

FIG. 1. The variation of the chain's (a) radius of gyration R_G, (b) squared ratio of the end-to-end distance R_E to R_G, and (c) contour length R_C with Debye parameter κ in bulk solution. The experimental data in (c) are from Chun and Park (Ref. 24). The range of κ corresponds to ionic strengths of 0.01–100 mM from left to right.

Model B well reproduces the experimental data[24] available at $\kappa^{-1} \leqslant 21$ nm ($I \geqslant 0.2$ mM). We point out that l_P^n varies significantly with n at large κ^{-1} (small I), with larger value for larger n. For example, model B shows $l_P^1 = 534$ nm and $l_P^{15} = 1076$ nm at the largest κ^{-1} [Fig. 2(b)], while they are identical for $\kappa^{-1} \leqslant 4.8$ nm. Although not presented here, the persistence lengths for $n \geqslant 10$ are all virtually identical. Therefore, the electrostatic interaction strengthens the long-range bond vector correlation to a larger degree than the short length scale correlation, in qualitative agreement with the theoretical analysis of Barrat and Joanny.[17]

Figure 2 also shows the theoretical predictions according

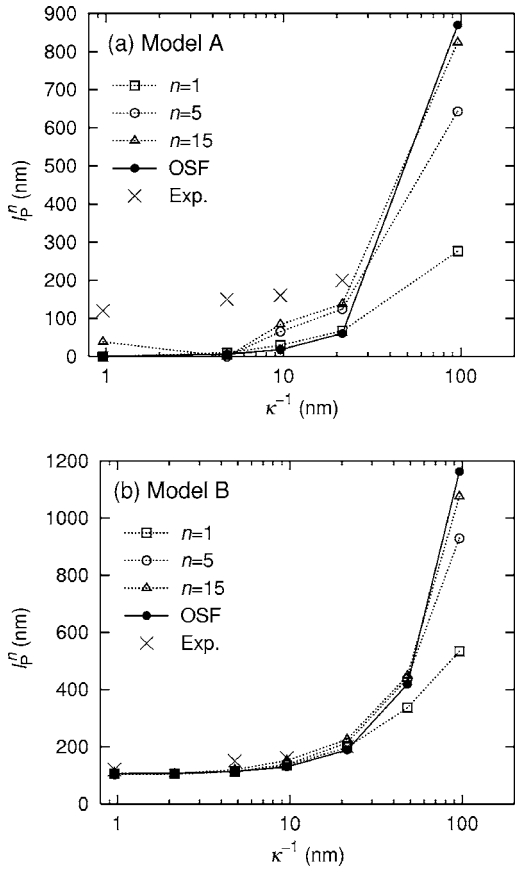

FIG. 2. Persistence length l_P^n as a function of the Debye screening length κ^{-1}. l_P^n corresponds to the correlation length of bond vectors separated by n bonds. The entry "OSF" is a theoretical prediction according to the modified OSF theory. The experimental data labeled "Exp." are from Chun and Park (Ref. 24). See text for details.

to Odijk, Skolnick, and Fixman (OSF).[38,39] Since the current models allow for changes in contour length, unlike the wormlike chain model employed in the OSF theory, we use the following expression:

$$l_P = l_P^0 + l_P^{\mathrm{el}}, \quad l_P^{\mathrm{el}} = \frac{l_B}{4 l_q^2 \kappa^2} = \frac{l_B (z_b N_b)^2}{4 R_C^2 \kappa^2}, \tag{14}$$

where l_P^0 is the intrinsic persistence length and the contour distance per unit charge l_q is written explicitly in terms of the varying contour length R_C. The resulting data in Fig. 2 demonstrate a fair overall agreement with the simulation results. In particular, the OSF theory agrees better with short-range l_P^1 at $\kappa^{-1} \leqslant 21$ nm ($I \geqslant 0.2$ mM), while at larger κ^{-1}, it is closer to the long-range value l_P^{15}.

The self-diffusion coefficient provides additional important information on the chain structure as well as dynamics. In bulk solution, the full 3D diffusion coefficient is found to differ from the two-dimensional (2D) one with only x and y components by less than 2%, but this is significant in the evaluation of confinement effect on diffusion. Thus, to better compare the bulk diffusion with that of a confined chain, we focus on the 2D diffusion coefficient in bulk. Figure 3 shows the ionic strength dependence of the self-diffusion coefficient of chain D_T^{2D} in bulk solution. As expected, D_T^{2D} increases with increasing κ since the chain becomes more compact at high ionic strength. The values for each model converge to

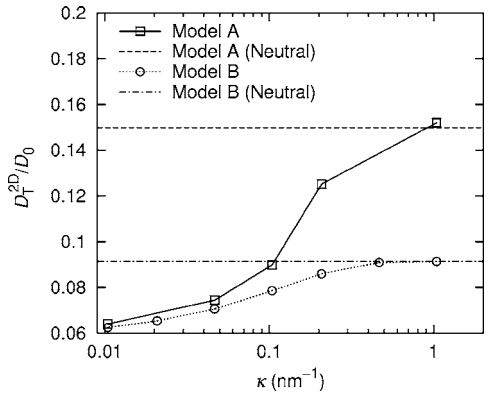

FIG. 3. Self-diffusion coefficients of a single polyelectrolyte chain in bulk solution with varying medium ionic strength. As explained in text, only the diffusion in x and y directions is included in D_T^{2D} to better compare with the diffusion under confinement. The diffusion coefficient of a single bead $D_0 = k_B T/(6\pi\eta a)$ is given as 4.91×10^{-11} m^2 s^{-1}.

~6% of the single bead value D_0 at small κ. The large difference in D_T^{2D} between two models at high κ can be attributed to the size difference shown in Fig. 1. We note that the diffusion becomes more than three times slower without the Rotne-Prager hydrodynamic interaction, because the latter interaction enhances the collective motion of beads.

B. Effect of confinement on chain conformation and diffusion

In Figs. 4(a) and 5(a), R_G of confined chains, scaled by the corresponding bulk values, are plotted with varying slit half-width Z_0 for models A and B. They show a distinct

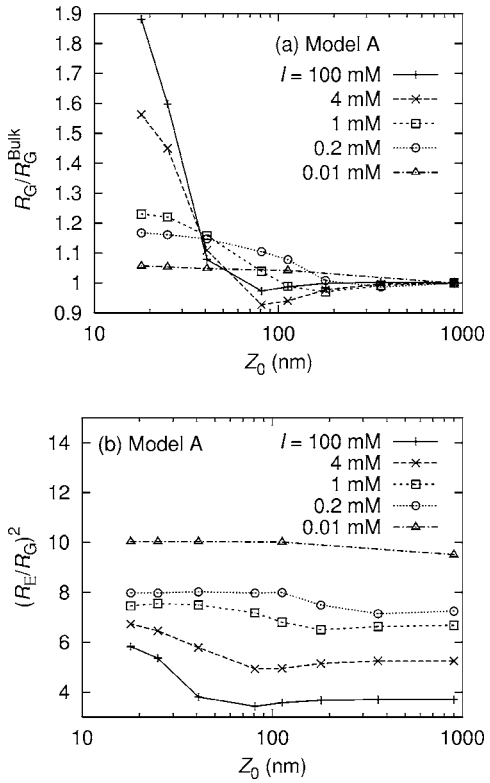

FIG. 4. The structural change of a confined flexible chain (model A) with varying half slit width Z_0. (a) Radius of gyration R_G relative to the bulk value and (b) squared ratio of the end-to-end distance R_E to R_G are shown.

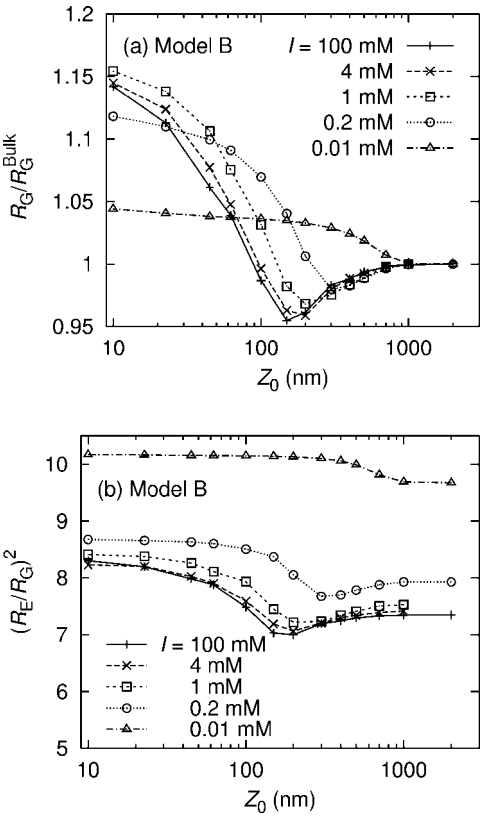

FIG. 5. The structural change of a confined semiflexible chain (model B) with varying half slit width Z_0. (a) Radius of gyration R_G relative to the bulk value and (b) squared ratio of the end-to-end distance R_E to R_G are shown.

minimum at Z_0=70–200 nm for model A as the medium ionic strength changes between 1 and 100 mM. For model B, a similar minimum in R_G is found with its location varying in the range Z_0=150–300 nm as I changes from 0.2 to 100 mM. At smaller I (i.e., I=0.01 and 0.2 mM for model A, and I=0.01 mM for model B), the minima are suppressed and the chain exhibits a sigmoidal transition instead. As the medium ionic strength increases, the minima or transition points appear at a larger Z_0. Very similar behavior is observed for the end-to-end distance R_E, however, relative variations are larger (in this regard, see Fig. 10).

As plotted in Figs. 4(b) and 5(b), the behavior of $(R_E/R_G)^2$ clearly shows that the influence of confinement is more severe for R_E than for R_G. Comparing this result with the bulk structural parameters in Table II, it is found that the minima or transitions in size appear when the slit width $2Z_0$ is slightly larger than the bulk end-to-end distance R_E at the same ionic strength. Thus, chain ends are first influenced by the confining walls, and their primary effect is to decrease R_E and, to a lesser degree, R_G. Although not studied here, the rotational diffusion of a confined chain would reflect this effect sensitively. As the channel further narrows down, the chain begins to extend rapidly until it converges to a 2D structure in the limit $Z_0\rightarrow0$. We note that the reduction of structural parameters R_G, R_E, and $(R_E/R_G)^2$ in Figs. 4, 5, and 10 is most pronounced at high ionic strength and gradually disappears as I decreases (with one exception of model A at I=100 mM, where the size parameters at the minimum are slightly larger than at I=4 mM). This suggests that the size-

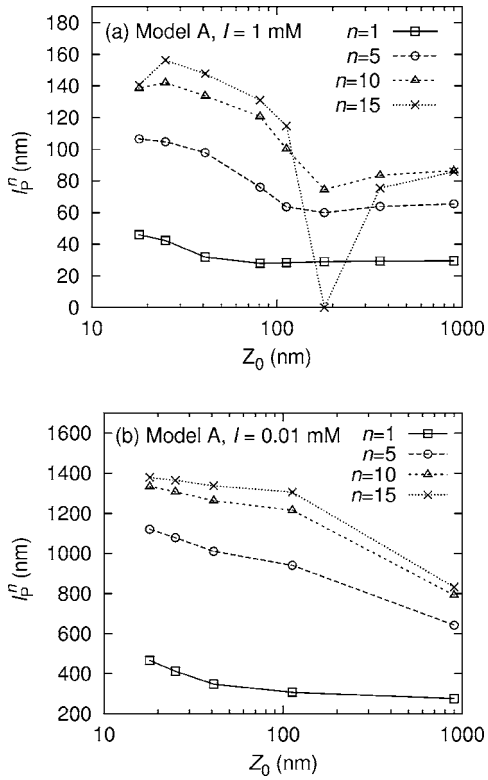

FIG. 6. Dependence of persistence length l_P^n of a confined flexible chain (model A) on the half slit width Z_0. Results at ionic strengths of (a) 1 mM and (b) 0.01 mM are shown.

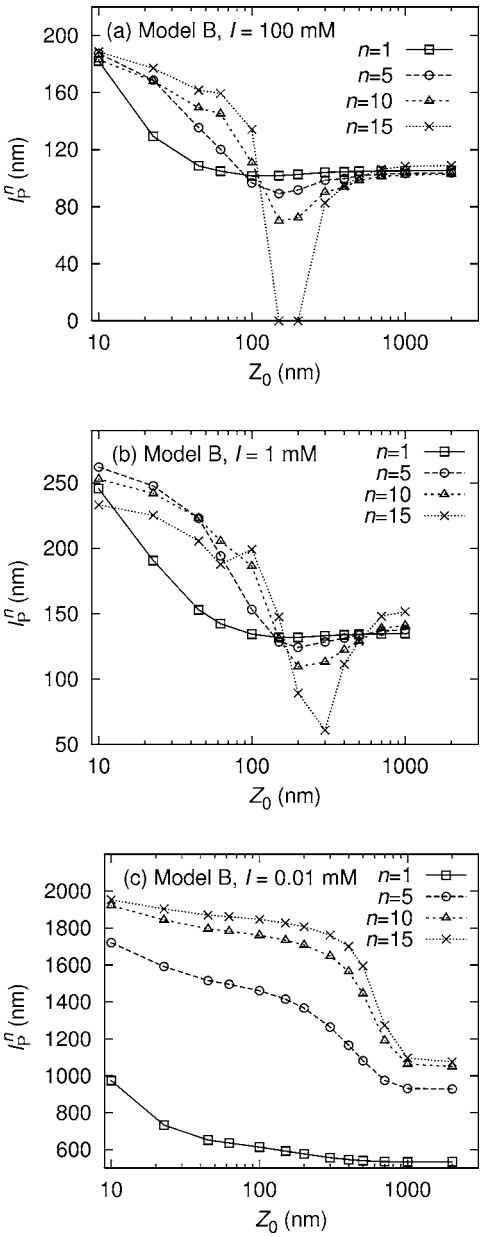

FIG. 7. Dependence of persistence length l_P^n of a confined semiflexible chain (model B) on the half slit width Z_0. Results at ionic strengths of (a) 100 mM, (b) 1 mM, and (c) 0.01 mM are shown.

reducing effect of confinement is largest in the more flexible chains with small rigidity. This effect becomes less important as the chain rigidity grows with increasing I and disappears altogether in the rigid rod limit at high I.

Confinement also affects the bond vector correlation and the persistence length. In Figs. 6 and 7, the distance-dependent persistence length l_P^n is shown for each model as a function of half slit width Z_0. In general, l_P^n increases with decreasing Z_0. However, as in the case of R_G, this transition is not monotonic at intermediate to high ionic strengths. For example, Fig. 6(a) shows a complete loss of long-range bond vector correlation (for $n=15$) and a small dip (for $n=10$) at $Z_0 \cong 200$ nm and $I=1$ mM. In contrast, short-range l_P^n ($n=1,5$), as well as all cases at low I [Fig. 6(b)], exhibit a sigmoidal transition without minimum. The absence of a minimum at low I has also been observed in other structural parameters in Fig. 4. The semiflexible chain (model B) exhibits a similar nonmonotonic behavior of long-range l_P^n at high ionic strengths $I=100$ and 1 mM [Figs. 7(a) and 7(b)], while it assumes a sigmoidal behavior at low I [Fig. 7(c)]. Comparisons of Figs. 5 and 7, as well as of Figs. 4 and 6 reveal that all three structural parameters, R_G, $(R_E/R_G)^2$, and l_P^n, share the same location of minimum or sigmoidal transition. Figures 6 and 7 also show a large difference in l_P^n between the small and large Z_0 limits, with their ratio varying between 1.5 and 2. This is due to a structural transition from the bulk to the two-dimensional chain with significant stiffening. For a wormlike chain with bending potential alone, it has been known that the persistence length and the stiffness parameter k are related as $l_P=2k/[(d-1)k_BT]$, where d is the system dimensionality.[33] For a fixed k, a strongly confined chain with 2D character is accordingly expected to have twice the persistence length of a 3D chain, close to the values found here.

The large difference between the short- and long-range bond vector correlations, exhibited by the difference in l_P^n at large and small n and observed at small ionic strengths in the bulk solution (Fig. 2), is carried over to the confined situation. This is demonstrated by the ratio l_P^{15}/l_P^1 as a function of Z_0, shown in Fig. 8. The ratio l_P^{15}/l_P^1 in the large Z_0 limit is in the range between 2 and 3 for model A and between 1 and 2 for model B, where bond vector correlations are nonexponentially decayed. Remarkably, these ratios are maintained in the strong confinement (small Z_0) limit despite a wide variation at intermediate Z_0. Thus, strong confinement affects the

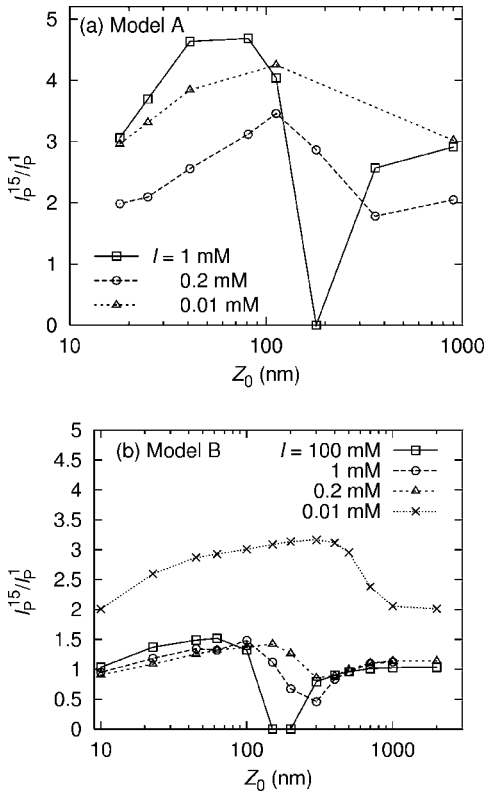

FIG. 8. The strength of the long-range bond vector correlation of a confined polyelectrolyte relative to the short-range correlation, as measured by the ratio of the distance-dependent persistence lengths l_P^{15}/l_P^1.

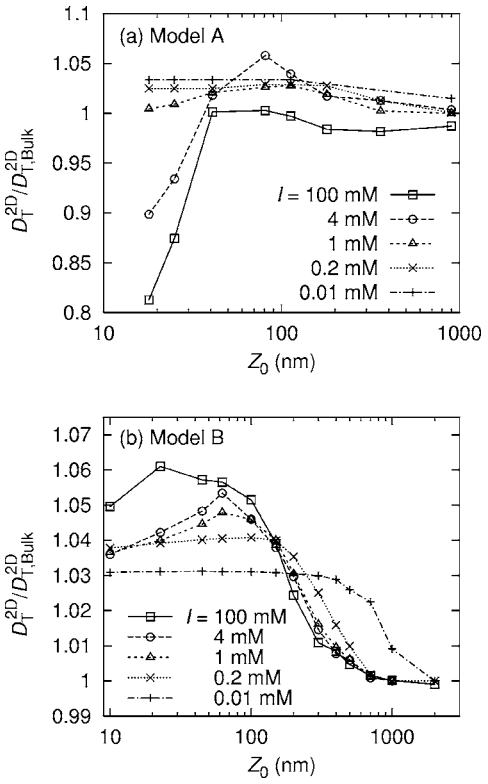

FIG. 9. Two-dimensional diffusion coefficient D_T^{2D} of a confined polyelectrolyte, scaled by the corresponding bulk value, as a function of the half slit width Z_0. Results for (a) flexible model A and (b) semiflexible model B are shown. D_T^{2D} only reflects displacement parallel to the walls.

short- and long-range bond vector correlations to a similar extent although their responses in the intermediate confinement regime are quite different.

As a representative dynamics, two-dimensional diffusion coefficients D_T^{2D} of a confined polyelectrolyte are presented in Fig. 9 with varying Z_0. To reveal the effect of confinement, they are scaled by the corresponding bulk value (cf. Fig. 3). For model A in Fig. 9(a), the flexible chains at high I exhibit a slightly faster diffusion at intermediate Z_0 before slowdown by 10%–20% in the strong confinement limit. In contrast, chains with finite rigidity at smaller I show a gradual increase in D_T^{2D} of up to 2%–3%. The results for model B in Fig. 9(b) show a similar behavior, except that D_T^{2D} is now always greater than its bulk counterpart. At first glance, this enhanced 2D diffusivity is surprising because the chain becomes more extended with larger R_G and $(R_E/R_G)^2$ with decreasing wall separation (cf. Figs. 4 and 5). The only possibility seems to be the anisotropy in chain extension, where the cross-sectional area of a confined chain is different when projected to the plane perpendicular to the walls than when projected to the wall plane. If such a projected area is smaller than that in the free chain, the diffusion in the direction perpendicular to that plane would become faster, as observed here in semiflexible chains. The fact that enhanced diffusivity is not observed in flexible chains supports this explanation because, in flexible chains, the free chain already has a very small cross-sectional area with a high degree of compaction and therefore would yield a larger projected area no matter how much extended. From these considerations, we can conclude that the structural contribution to the hindered diffusion of a polymer chain is significant only with *flexible* chains and that confinement can actually enhance diffusion to a small extent in *semiflexible* chains.

We emphasize that the present result does not take into account the hindrance to diffusion arising from the wall-bead hydrodynamic interaction. The present result shows that any hindered diffusion observed in semiflexible or wormlike chains would be solely due to such hydrodynamic interactions, while in flexible chains the structural and hydrodynamic effects can add up to slow down the diffusion of a confined polymer.

V. CONCLUDING REMARKS

We have developed coarse-grained chain models of intrinsically flexible and semiflexible polyelectrolytes with the anionic polysaccharide xanthan as the target system. BD simulations with the models in bulk solutions and under confinement in a slit channel between two parallel plates revealed an interesting crossover behavior from the 3D chain to a 2D one. Here, we make a brief analysis of the results in terms of existing theoretical formula for wormlike chains and summarize major findings.

Both in 2D and 3D spaces, the end-to-end distance of a wormlike chain is related to its contour length R_C and the persistence length l_P (Refs. 37 and 40) as follows:

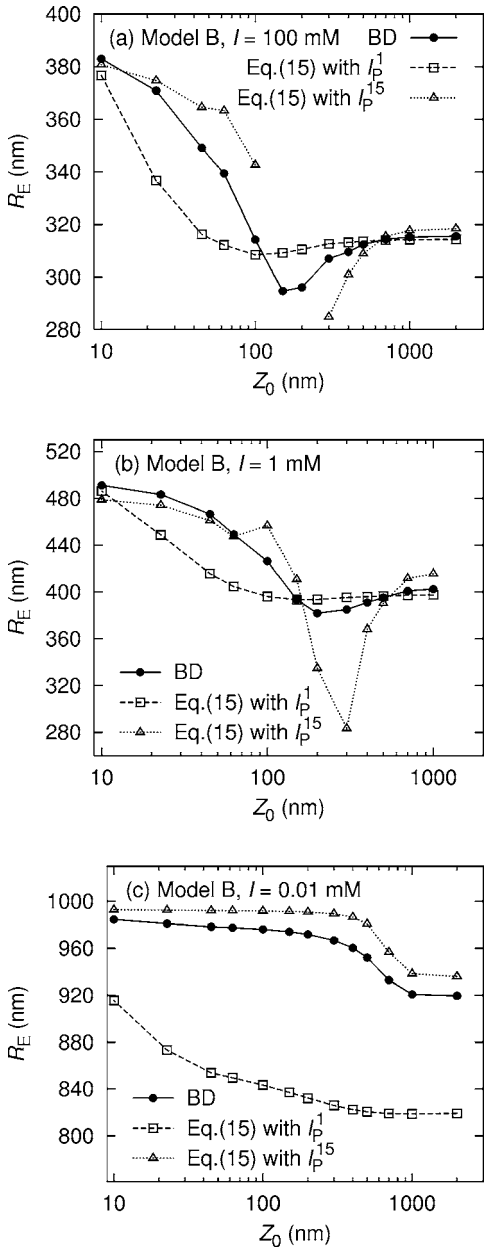

FIG. 10. Variation of the end-to-end distance of a semiflexible polyelectrolyte (model B) with the half slit width Z_0. Results at ionic strengths of (a) 100 mM, (b) 1 mM, and (c) 0.01 mM are presented. Corresponding theoretical predictions according to Eq. (15) are also shown. The simulation results for the contour length R_C and the persistence length l_P^n were used in the evaluation of R_E in Eq. (15).

$$R_E^2 = 2(R_C/l_P - 1 + e^{-R_C/l_P})l_P^2. \tag{15}$$

However, as discussed earlier, l_P of a 2D wormlike chain is twice that of a 3D chain and the resulting R_E will be different. This suggests that Eq. (15) will hold both in the bulk and in the strong confinement limit if proper values of l_P are supplied. Figure 10 compares R_E from BD simulations and Eq. (15) at different ionic strengths as a function of the slit half-width Z_0. As expected, the simulation and theoretical values evaluated with long-range l_P^{15} agree well with the simulation results in the large and small Z_0 limits. Moreover, the location of minima or transition at intermediate Z_0 is well reproduced although the depth of the minima is overestimated by the theoretical formula. On the other hand, the theoretical value with short-range l_P^1 shows a poor agreement with the simulation. This clearly provides that structural transition of a confined polyelectrolyte is strongly coupled to the strength of the long-range bond vector correlation. It also tells us that the role of electrostatic interaction and medium ionic strength can reasonably be captured by the persistence length. In other words, once the variation in persistence length due to electrostatics is taken into account, the wormlike chain model is suitable for evaluating the size of semiflexible polyelectrolytes.

This study demonstrates that the nonmonotonic crossover behavior of an intrinsically flexible polymer[7–9] under confinement in a slit channel is carried over to semiflexible chains with intrinsic persistence length. Unlike flexible chains, however, semiflexible chains show a severe loss of long-range bond vector correlation in addition to the reduction in size at intermediate slit widths. Thus, for semiflexible chains, the structural transition upon confinement can be summarized as the following three-step process. Initially, the rotationally diffusing chain interacts with the approaching walls, mainly through its terminal beads, decreasing in size and simultaneously losing long-range bond vector correlation. This takes place when the slit width $(2Z_0)$ becomes less than 1.5 times the end-to-end distance of the chain in bulk solution. Second, upon further confinement until $2Z_0$ falls below R_G, the chain begins to extend and the long-range persistence length is recovered. At this stage, the overall chain size becomes larger than in the bulk but is still smaller than that of a strongly confined chain. In terms of the bond vector correlation, this is the region where the long-range correlation increases while the short-range correlation has not yet responded, leading to a large ratio between the two. Finally, as the slit further narrows down, the short-range correlation begins to increase as well and the chain converges to a structure suitable in reduced spatial dimensions.

In the low ionic strength limit ($I \leqslant 0.01$ mM), however, polyelectrolytes exhibit persistence lengths as large as their contour lengths and thus can be classified as rigid. For these rigid chains, the first step above, namely, the reduction in size and loss of long-range correlation, is not important and the structural transition becomes a two-step process beginning with the second stage above. A third class of chains (model A at $I > 4$ mM) does not have a well-defined persistence length and is flexible in nature. These chains follow the three-step transition similar to the process[8,13] of van Vliet *et al.* without the variations of persistence length at long length scale.

A given polyelectrolyte chain will belong to one of the three classes of polyelectrolytes defined above, depending on the chain intrinsic rigidity, charges on chain, and medium ionic strength. Another factor that may influence the chain characteristics is the distance between beads. In the current models with 25 beads, the average bead-bead distance b lies between the Debye screening lengths at I=0.2 and 0.01 mM. Therefore, the discrete nature of the model can potentially affect the chain rigidity around these ranges of ionic strength due to a possible discontinuity in the screening of electrostatic interaction. Although this aspect is not relevant to the

scope of the present study, it needs to be carefully examined if a precise boundary is to be drawn between the semiflexible and rigid regimes of polyelectrolytes.

ACKNOWLEDGMENTS

This work was supported by the Basic Research Fund (No. R01-2004-000-10944-0) from the Korea Science and Engineering Foundation (KOSEF), as well as the Future-Oriented μTAS Research Fund (No. 2E19570) from the Korea Institute of Science and Technology (KIST).

[1] D. A. Hoagland and M. Muthukumar, Macromolecules **25**, 6696 (1992).
[2] R. M. Jendrejack, D. C. Schwartz, M. D. Graham, and J. J. de Pablo, J. Chem. Phys. **119**, 1165 (2003).
[3] Y.-L. Chen, M. D. Graham, J. J. de Pablo, G. C. Randall, M. Gupta, and P. S. Doyle, Phys. Rev. E **70**, 060901R (2004).
[4] P.-G. de Gennes, *Scaling Concepts in Polymer Physics* (Cornell University Press, Ithaca, 1979).
[5] I. Teraoka, Prog. Polym. Sci. **21**, 89 (1996).
[6] M. Daoud and P.-G. de Gennes, J. Phys. (France) **38**, 85 (1977).
[7] C. E. Cordeiro, M. Molisana, and D. Thirumalai, J. Phys. II **7**, 433 (1997).
[8] J. H. van Vliet and G. ten Brinke, J. Chem. Phys. **93**, 1436 (1990).
[9] Y. Wang and I. Teraoka, Macromolecules **33**, 3478 (2000).
[10] Y. Wang, J. Chem. Phys. **121**, 3898 (2004).
[11] V. Yamakov and A. Milchev, Phys. Rev. E **55**, 1704 (1997).
[12] G. Morrison and D. Thirumalai, J. Chem. Phys. **122**, 194907 (2005).
[13] J. H. van Vliet, M. C. Luyten, and G. ten Brinke, Macromolecules **25**, 3802 (1992).
[14] F. Brochard-Wyart, T. Tanaka, N. Borghi, and P.-G. de Gennes, Langmuir **21**, 4144 (2005).
[15] T. Odijk, Macromolecules **16**, 1340 (1983).
[16] W. Reisner, K. J. Morton, R. Riehn, Y. M. Wang, Z. Yu, M. Rosen, J. C. Sturm, S. Y. Chou, E. Frey, and R. H. Austin, Phys. Rev. Lett. **94**, 196101 (2005).
[17] J.-L. Barrat and J.-F. Joanny, Adv. Chem. Phys. **94**, 1 (1996).
[18] A. V. Dobrynin and M. Rubinstein, Prog. Polym. Sci. **30**, 1049 (2005).
[19] L. Bezemer, J. B. Ubbink, J. A. de Kooker, M. E. Kuil, and J. C. Leyte, Macromolecules **26**, 6436 (1993).
[20] H.-C. Lee and D. A. Brant, Macromolecules **35**, 2212 (2002).
[21] G. Paradossi and D. A. Brant, Macromolecules **15**, 874 (1982).
[22] T. Sato, T. Norisuye, and H. Fujita, Macromolecules **17**, 2696 (1984).
[23] T. Sho, T. Sato, and T. Norisuye, Biophys. Chem. **25**, 307 (1986).
[24] M.-S. Chun and O. O. Park, Macromol. Chem. Phys. **195**, 701 (1994).
[25] D. L. Ermak and J. A. McCammon, J. Chem. Phys. **69**, 1352 (1978).
[26] H. R. Warner, Jr., Ind. Eng. Chem. Fundam. **11**, 379 (1972).
[27] B. T. Stokke, A. Elgsaeter, G. Skjåk-Brjek, and O. Smidsrød, Carbohydr. Res. **160**, 13 (1987).
[28] T. A. Camesano and K. J. Wilkinson, Biomacromolecules **2**, 1184 (2001).
[29] T. M. McIntire and D. A. Brant, Biopolymers **42**, 133 (1997).
[30] G. S. Manning, J. Chem. Phys. **51**, 924 (1969).
[31] J. Hendricks, T. Kawakatsu, K. Kawasaki, and W. Zimmermann, Phys. Rev. E **51**, 2658 (1995).
[32] H. Jian, A. V. Vologodskii, and T. Schlick, J. Comput. Phys. **136**, 168 (1997).
[33] A. Dhar and D. Chaudhuri, Phys. Rev. Lett. **89**, 065502 (2002).
[34] M. X. Fernandes, M. L. Huertas, M. A. R. B. Castanho, and J. Garcia de la Torre, Biochim. Biophys. Acta **1463**, 131 (2000).
[35] M.-S. Chun and S. Lee, Colloids Surf., A **267**, 86 (2005).
[36] J. Rotne and S. Prager, J. Chem. Phys. **50**, 4831 (1969).
[37] M. Doi and S. F. Edwards, *The Theory of Polymer Dynamics* (Clarendon, Oxford, 1986).
[38] T. Odijk, J. Polym. Sci., Polym. Phys. Ed. **15**, 477 (1977).
[39] J. Skolnick and M. Fixman, Macromolecules **10**, 944 (1977).
[40] M. Fujii, J. Shimada, and H. Yamakawa, J. Polym. Sci., Polym. Phys. Ed. **12**, 1327 (1974).